SHALLOW-WATER FLOW AROUND MODEL CONICAL ISLANDS OF SMALL SIDE SLOPE. II: SUBMERGED

By Peter M. Lloyd[1] and Peter K. Stansby[2]

ABSTRACT: Experiments have been conducted to study the unsteady wakes of submerged conical islands. The islands used in the tests have side slopes ranging from 8.0 to 33.1°. Experiments in a shallow-water channel with a steady, subcritical free stream showed vortex shedding to occur in the wake when the water depth above the island apex was relatively small. Flow separation from positions near the island apex was found to be important in producing this unsteady wake. As the water depth was increased the shedding was observed to become less vigorous and eventually stop. All islands tested produced similar results with the angle of the island side slope exerting relatively little influence on the process. The results of wind tunnel visualization studies, which used a rigid top plate to produce the effect of fluid depth, support the results from the water channel. Pictures of the surface flow patterns produced on the islands by the wind action are presented. Two-dimensional (2D) and three-dimensional (3D) shallow-water numerical models with the hydrostatic pressure assumption have been run for comparison with the laboratory measurements. The complex 3D flow observed in the near wake provides a severe test for the models. Although both models were found to reproduce gross features of the submerged island wakes their mode of generation could be quite different in model and experiment.

INTRODUCTION

In Part I a series of laboratory experiments and numerical model simulations was undertaken to investigate the recirculating nature of shallow-water flow in the wakes of surface-piercing conical model islands with gently sloping sides. In Part II we consider the flow over and in the wake of submerged bodies. Sand mounds and tidal banks are often formed in shallow coastal waters (Pingree and Maddock 1979). Their effect on the general flow field and sediment processes, including the dynamics of their own formation and erosion, is of interest. Engineers in charge of managing coastal reaches require extensive information on a region's morphology when, for example, locating breakwaters or planning dredging operations. Another type of submerged body is commonly found in coastal stretches of warm water in the form of coral reefs. As well as increasing the vertical mixing levels in a water column, isolated coral reefs can produce large-scale zones of recirculation downstream of their mass. This was demonstrated in studies by Wolanski et al. (1984) and Hammer and Hauri (1981), both conducted in the coral-rich coast off northeastern Australia. The effects of the recirculating flow and increased turbulent mixing on the biological makeup of the region are discussed by the latter authors.

Relatively little published work exists that examines the wakes of submerged islands or shoals subject to a steady current. In deep ocean environments large seamounts, typically lying several kilometers beneath the water surface, can be a feature of the bottom topography. These seamounts have been found to modify the local current patterns producing downstream recirculating eddies, which have been modeled by Huppert and Bryan (1975). Current acceleration above their peaks has been found to alter the local biological conditions. Genin et al. (1986) observed an abundance of coral in regions of accelerated flow, attracted by the increased rate of suspension feeders. Relevant research concerned with the shallow-water environment appears to be even more scarce although studies of flow processes about two-dimensional (2D) structures such as sand dunes and ripples are available (Engel 1981).

Research into the flow about bodies submerged in a fluid is more commonly found in atmospheric studies. Although a large proportion of this type of work has concentrated on wind loading and flow dynamics about bluff bodies representative of buildings, there has been considerable interest in the interaction between atmospheric flows and complex terrain with hilly topographies. As noted by Snyder (1985), industrial sites and other sources of air pollution are often located within regions of complex terrain. In the laboratory, the flow about hills has been studied with varying model geometries and fluid parameters. Arya et al. (1987) measured turbulent velocity characteristics and tracer concentration levels downwind of 2D model hills in a meteorological wind tunnel. The separated flow region in the lee of a three-dimensional (3D) hill is more complex than that behind a 2D ridge. The fluid can now flow around and separate from the sides of the hill. Streamlines separating from near the apex of a 3D hill can descend into the wake before moving downwind. Arya and Gadiyaram (1986) examined far-field wake velocities and dispersion characteristics of two conical model hills with side slope angles of 26.5 and 17.5° in a meterological wind tunnel. Separation was observed from both models, with evidence of vortex shedding occurring in the wake of the steeper hill. Details of the shedding characteristics were not given. Several studies have concentrated on the dynamics of flow around 3D hills when the atmosphere is stratified. When stratification is strong the air flows in well-defined horizontal layers around the obstacle, with vortex shedding occurring in the wake (Brighton 1978). Although atmospheric boundary layer flows differ in many ways to the shallow free surface flows that are of interest in this project, under certain conditions (e.g., beneath inversion layers) the flows can possess similar features.

In this paper results are presented that examine shallow-water flow over submerged model "islands." Emphasis is placed on determining the wake patterns produced by the models as the angle of their side slope and the level of the water depth are altered. To our knowledge, experiments of a similar nature have not been conducted previously. The test series should therefore provide valuable new information on the effect of an isolated rise in the bed bathymetry on a subcritical shallow open channel flow.

The 2D and 3D finite-difference models based on the shallow-water equations have been run for comparison with the experimental data. Although vertical velocities are ignored in

[1]Res. Assoc., Hydrodynamics Res. Group, The Manchester School of Engrg., Univ. of Manchester, Manchester M13 9PL, U.K.

[2]Prof. of Hydrodynamics, Hydrodynamics Res. Group, The Manchester School of Engrg., Univ. of Manchester, Manchester M13 9PL, U.K.

Note. Discussion open until May 1, 1998. Separate discussions should be submitted for the individual papers in this symposium. To extend the closing date one month, a written request must be filed with the ASCE Manager of Journals. The manuscript for this paper was submitted for review and possible publication on November 13, 1996. This paper is part of the ***Journal of Hydraulic Engineering***, Vol. 123, No. 12, December, 1997. ©ASCE, ISSN 0733-9429/97/0012-1068–1077/$4.00 + $.50 per page. Paper No. 12347.

depth-averaged models, 2D computations are used commonly to model shallow-water flows with complex bathymetries where, at certain locations, vertical velocities may be significant. The comparison carried out here provides information on the ability of 2D models to simulate such flows. Also 3D models are increasingly being used for shallow-water applications. However, uncertainties still persist in capturing the effects of turbulence and pressure is assumed to be hydrostatic so that vertical accelerations are ignored and flow separation in a vertical plane cannot be simulated [e.g., Johns (1991)]. Details of the numerical models can be found in Stansby and Lloyd (1995).

EXPERIMENTAL ARRANGEMENT

Experiments are conducted in a shallow-water flume with horizontal dimensions of 9.75 by 1.52 m. In the series of tests described here the fully developed free-stream flow was in a subcritical, smooth turbulent state. The flow is described by the depth Reynolds number, R_h given by

$$R_h = \frac{U_0 h}{\nu} \tag{1}$$

where U_0 = free-stream velocity; h = water depth; and ν is the kinematic viscosity. A summary of experimental conditions is listed in Table 1.

Periodic frequencies of the wake flows will be expressed by a nondimensional Strouhal number S, defined as

$$S = \frac{fD_a}{U_0} \tag{2}$$

where f = measured frequency; and D_a = island diameter at its midheight.

The four conical model islands described in Part I have also been used for the submerged study. Where θ is the slope angle (to the horizontal), "island 1" will denote the model with $\theta = 33.1°$, "island 2" with $\theta = 22.2°$, "island 3" with $\theta = 12.6°$, and "island 4" with $\theta = 8.0°$.

Surface velocity measurements have been made with a particle tracking velocimetry (PTV) system. This measures velocities by tracking the movement of small surface floating tracer particles (Lloyd et al. 1995). Consequently, the figures showing whole-field maps of the laboratory flow depict velocity vectors at the water surface.

TABLE 1. Summary of Experimental Conditions

Model (1)	Run (2)	U_0 (m/s) (3)	h (m) (4)	h/h_i (5)	R_h (6)
1	SB1_01	0.115	0.076	1.01	8,739
1	SB1_02	0.115	0.082	1.09	9,430
1	SB1_03	0.115	0.087	1.16	10,004
1	SB1_04	0.115	0.100	1.33	11,500
2	SB2_01	0.115	0.103	1.04	11,845
2	SB2_02	0.115	0.113	1.14	12,995
2	SB2_03	0.115	0.123	1.24	14,145
2	SB2_04	0.106	0.136	1.37	14,416
3	SB3_01	0.115	0.068	1.03	7,820
3	SB3_02	0.115	0.072	1.09	8,279
3	SB3_03	0.115	0.075	1.14	8,625
3	SB3_04	0.115	0.080	1.21	9,199
3	SB3_05	0.115	0.084	1.27	9,660
3	SB3_06	0.115	0.090	1.36	10,350
4	SB4_01	0.115	0.050	1.02	5,750
4	SB4_02	0.115	0.054	1.10	6,210
4	SB4_03	0.115	0.056	1.14	6,440
4	SB4_04	0.115	0.057	1.16	6,555
4	SB4_05	0.115	0.059	1.20	6,785
4	SB4_06	0.115	0.064	1.31	7,360

RESULTS

Experimental Measurements and Observations

Measurements of the surface velocities were made using the PTV system for all of the flow cases listed in Table 1. The tests were further visualized by injecting methylene blue dye into the flow upstream of the model position. Further information on selected tests was obtained using potassium permanganate crystals ($KMnO_4$) and small plastic flow "vanes" free to rotate about a thin vertical wire in a horizontal plane. Pairs of these rigid vanes, one near the bed and the other just below the surface, were stationed at selected positions in the flow to provide information on the flow direction at the two depths.

Shown in Figs. 1(a–d) are pictures produced from digital images of the distribution of methylene blue dye in the wake of island 4 ($\theta = 8.0°$). The sequence shows the wake as the depth over the island is increased from $h/h_i = 1.02$ to $h/h_i = 1.20$. For all tests the mean velocity $U_0 = 0.115$ m/s. For the case with $h/h_i = 1.02$ [Fig. 1(a)], the flow was deflected around the upper shoulder of the model, with little water flowing over the apex into the near wake. A vigorous vortex shedding wake was formed, with flow recirculating close behind the model. The wake flow was periodic with S = 0.29. The frequency was measured by recording the average time period of the wake oscillation over a fixed number of cycles, either from video recordings of the dye or from the movement of water vanes. Increasing the flow depth to $h/h_i = 1.10$ [Fig. 1(b)] resulted in an accelerated flow region above the apex, causing the recirculating near-wake "bubble" and therefore the initiation of vortex shedding to move downstream of the island center (marked with a small dot on the images shown in Fig. 1). The wake narrowed and, although still clearly periodic, its frequency increased to give S = 0.34. With the flow depth increased to $h/h_i = 1.16$ [Fig. 1(c)] the wake bubble moved further downstream. The wake fluctuation was more irregular and a single frequency could not be identified. The shedding now appeared as long "fingers" of dye, emanating from the low-velocity region downstream of the island center. A further increase in the water depth resulted in the wake entirely losing its periodicity. Fig. 1(d) shows the wake with $h/h_i = 1.20$ to display no vortex shedding characteristics although small oscillations were observed in the far field. For greater fluid depths (h/h_i was increased up to 1.49 in the tests) a thin region of slow-moving fluid was always present in the wake, the dye becoming fainter and the wake narrower with a smaller velocity deficit as depth increased.

A "flushing time" T_f was defined as the time taken for a volume of dye to discharge from the saturated near-wake region, such that the pixel gray levels on the digital image returned to their original values, i.e., the gray level of the flume bed. The vigorous vortex shedding wake, with $h/h_i = 1.02$, entrained large quantities of "fresh" water, which quickly flushed out the dye, resulting in a relatively short residence time. It was described in the foregoing paragraph how increasing the flow depth caused the wake region to narrow and the vortex shedding system to weaken. This resulted in a gradual increase in the flushing time, taking 1.5 times longer for the case with $h/h_i = 1.14$ than for $h/h_i = 1.02$. However, the amount of dye trapped was relatively small and was concentrated in the small wake bubble (i.e., the low-velocity region in the near wake) downstream of the island center. With further increase in water depth, well-organized vortex shedding stopped and the flushing time began to decrease. For the case with $h/h_i = 1.20$ the formation of a wake bubble capable of trapping dyed water in the near-field region was less apparent. Dye caught in the wake drifted downstream in the slow-moving flow.

Surface velocity vector plots, obtained using PTV, are illus-

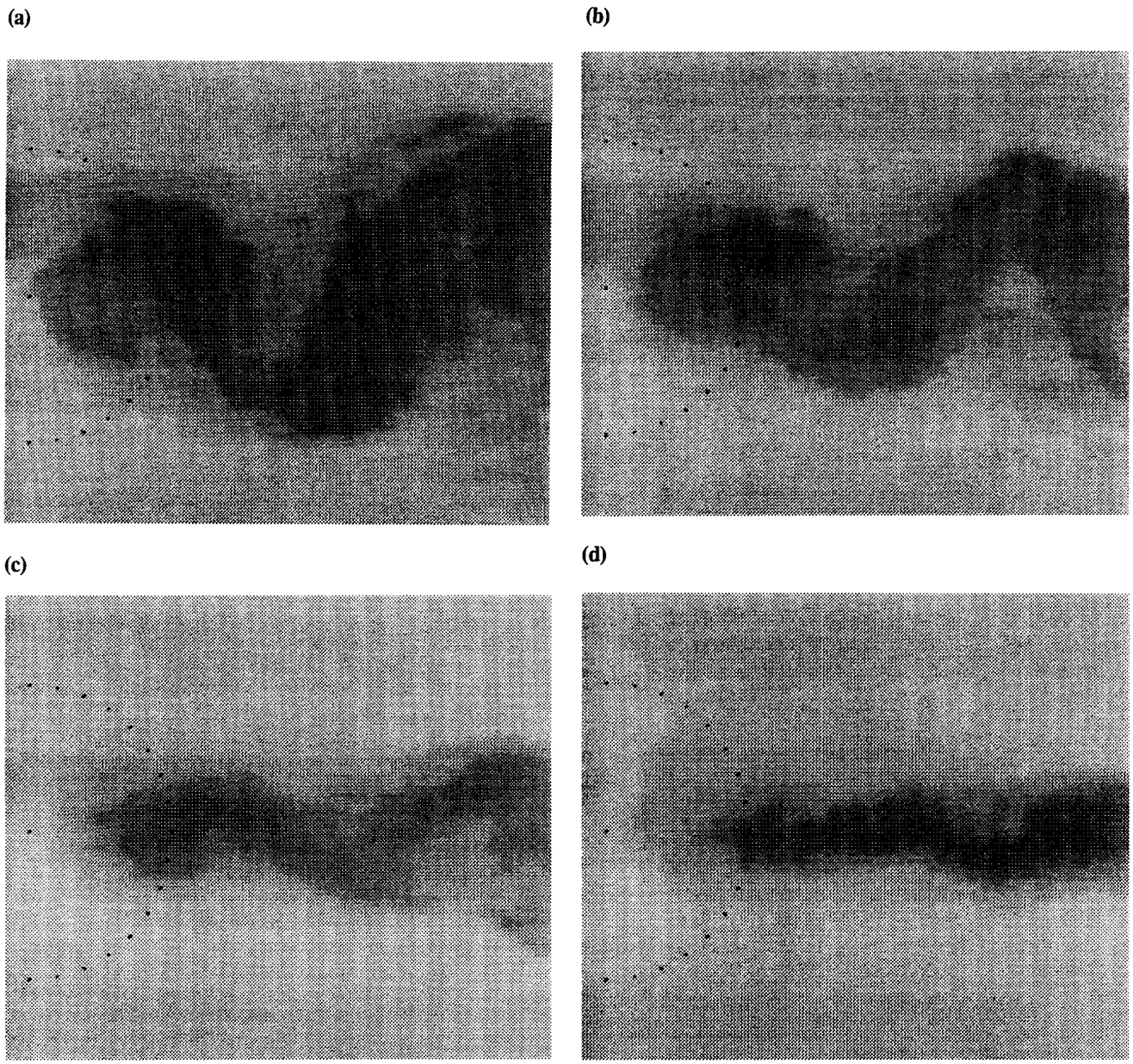

FIG. 1. Dye Visualization of Wake of Island 4 ($\theta = 8.0°$) with Value of h/h_i: (a) 1.02; (b) 1.10; (c) 1.16; (d) 1.20

trated in Figs. 2(a–d) for the cases shown in Figs. 1(a–d) with h/h_i = 1.02, 1.10, 1.16, and 1.20, respectively. The transition from a vortex shedding wake to a narrow low-velocity steady (or almost steady) wake flow without recirculation is clearly seen. These results concerning the wake of island 4 ($\theta = 8.0°$) have been presented as a representative example of the results found for all the models studied. For island 1 ($\theta = 33.1°$), island 2 ($\theta = 22.2°$), and island 3 ($\theta = 12.6°$), vortex shedding also decreased in strength and then ceased as the depth of water above the island increased. For island 1 the shedding ceased when $h/h_i \approx 1.13$ (10 mm above the apex), for island 2 when $h/h_i \approx 1.14$ (14 mm above apex), and for island 3 when $h/h_i \approx 1.17$ (11 mm above apex).

With the use of the visualization tools described in the foregoing paragraph ($KMnO_4$, dye and vanes), the structure of the unsteady island wakes was studied in more detail. The principal aim was to investigate the cause of the large-scale horizontal vortex shedding and the manner of its disappearance with increasing water depth. The $KMnO_4$ crystals were used to demarcate lines of separation on the surface of the model, with the methylene blue dye helping to visualize 3D structures in the near field. Because the four islands displayed similar wake characteristics, the following results will discuss a "general" case, with reference made to the model 4 study illustrated in Figs. 1(a–d) and 2(a–d).

With the water level at or just above the island apex [producing vortex shedding wakes similar to those shown in Figs. 1(a) and 2(a)], the separation mechanism was similar to that described in Part I for cases where the model island was surface piercing. There was little flow over the apex, with the island acting to shelter the near-field region. The vortex shedding wake was caused by interaction between shear layers formed between the low-velocity, sheltered near-field region and the accelerated flow around the sides of the island. Flow separation from near the upper shoulders resulted in a near wake that was well mixed across the depth. In this region the movement of vanes suggested a significant variation in the flow direction over the depth. Further downstream the vane movement was roughly in phase across the depth.

A small increase in the water depth resulted in more water flowing over the top of the island, producing a significant change to the mechanism causing large-scale vortex shedding.

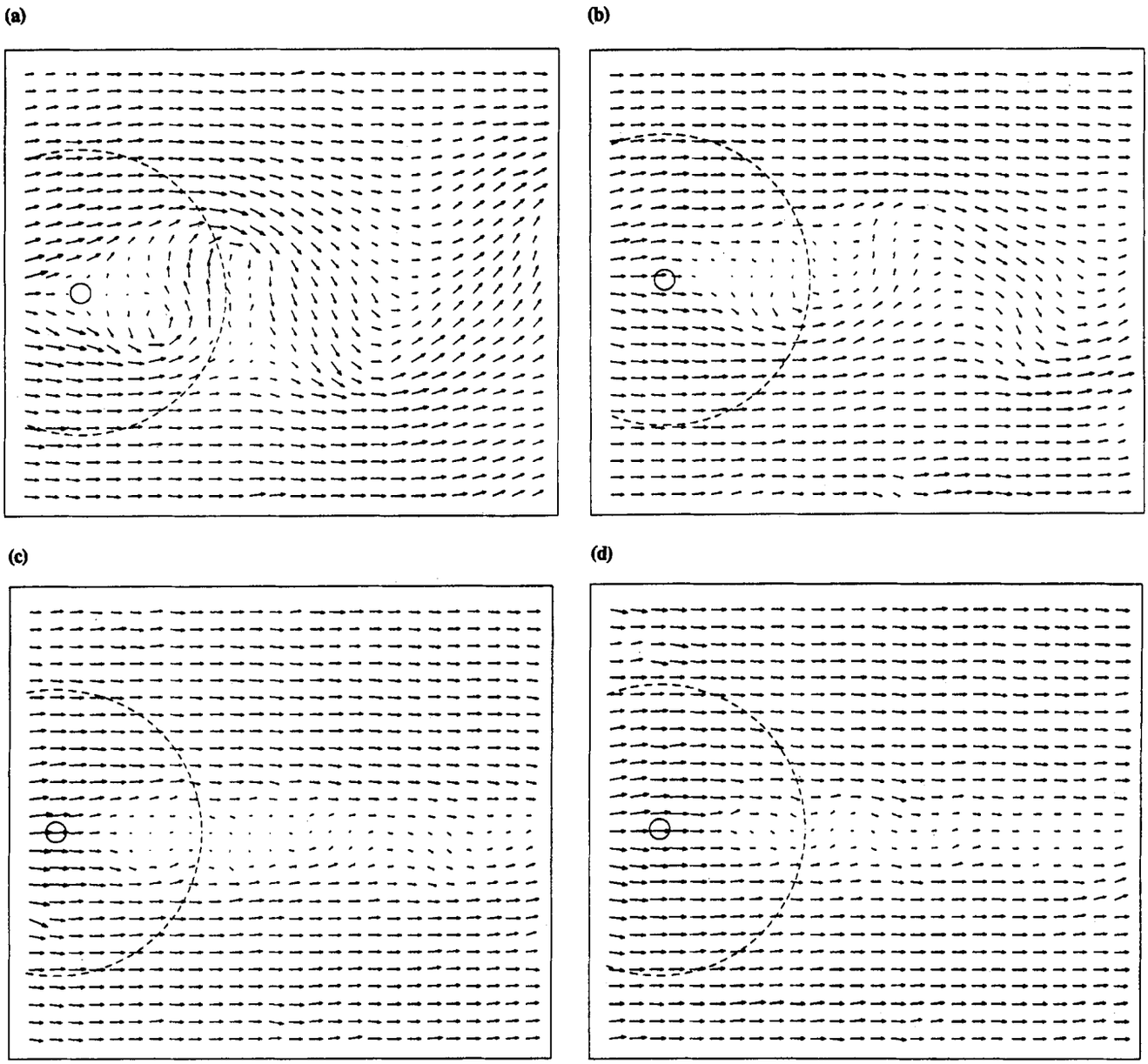

FIG. 2. Experimental Surface Velocity Vector Fields of Wake of Island 4 ($\theta = 8.0°$) with Value of h/h_i: (a) 1.02; (b) 1.10; (c) 1.16; (d) 1.20

It is seen in Fig. 1(b), where $h/h_i = 1.10$, how the introduction of this water into the near-wake region moves the initiation of shedding downstream, with the island no longer sheltering the near field so effectively. Although there was appreciable flow into the near field, well-organized periodic eddies were still a prominent feature of the downstream wake. The origin of the vortex shedding wake is separation of the narrow stream of accelerated flow close to the apex of the island. The flow separates from the downstream lip of the horizontal apex and from a narrow region across the upper shoulders. A sketch labeling these important features of the flow near the island is included in Fig. 3. This separation causes strong vertical mixing just downstream of the apex and results in a low-velocity region in the near wake (i.e., a velocity deficit is produced). The horizontal shear layers, generated between this low-velocity region and the unseparated flow over the shoulders of the island further away from the apex, produce the unsteady wake.

A further increase in the depth of the mean flow resulted in the low-velocity region in the near wake narrowing as the depth at positions near the upper shoulders became too large for the separated fluid to mix throughout the depth. The reduced wake with the increased mass flux above the island acted to reduce the velocity deficit in the near wake, producing less energetic vortex shedding. At a certain depth (e.g., $h/h_i \approx 1.18$ for island 4 with $U_0 = 0.115$ m/s) the near-wake width and velocity deficit become too small to generate well-organized vortex shedding, although relatively small high-frequency eddies could be present in the wake.

This process of transition, from vortex shedding to an almost steady state, shares similarities with the "base-bleed" technique used in aerodynamic studies on the control of the form of the wake flow behind aerofoils (Wood 1964). With this technique, fluid is injected into the near-field region, reducing the velocity deficit in the wake to stop or delay the onset of large-scale vortex shedding. A similar effect can be produced by a porous plate. Chen and Jirka (1995) conducted a series of experiments looking at the suppression of vortex shedding in the wake of a porous plate positioned in a shallow-water layer.

Observations of the bed flow visualized with $KMnO_4$ tracers revealed lines of separation extending down toward the base

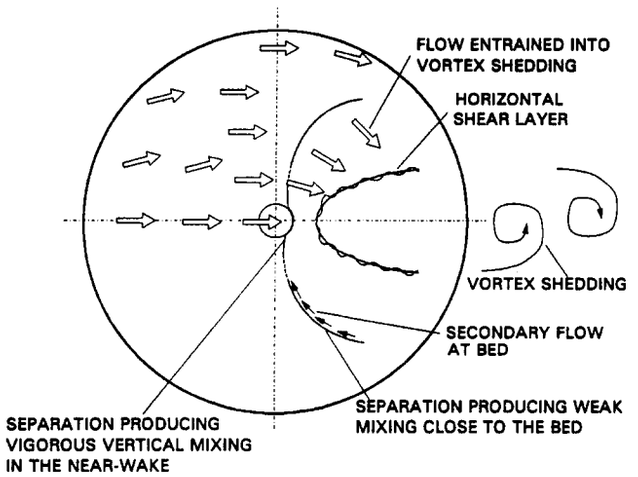

FIG. 3. Sketch of Near-Field Wake Flow

perimeter of the island. In contrast to separation from near the apex, which produced mixing throughout the depth, separation from positions along the middle and lower portions of the island's shoulders produced a relatively local effect with mixing observed close to the bed only. Although the $KMnO_4$ tracers on the island surface clearly separated from the body, dye released a short distance above the bed was observed to follow the same path as dye released at the water surface. A secondary flow was clearly observed along the separation lines on the island shoulders. In general there was little evidence (from observations of water vanes along the wake centerline) of a significant depthwise variation in the flow direction at far-wake positions.

The $KMnO_4$ crystals visualized primary lines of separation and secondary currents but other possible interesting details (e.g., attachment and secondary separation lines), particularly in highly turbulent or low-velocity regions, were not visible. When filmed from above many details were blurred by dye streaks separating from the body and mixing with the unseparated flow above. Although useful for visualizing the large-scale wake vortices, these dye traces away from the model surface concealed the flow pattern at the bed.

A more established and reliable technique for producing the flow pattern on the surface of a model is the oil-film evaporation method, traditionally used in wind tunnel studies [e.g., Nakayama (1988)]. With this method the model is thinly coated with a mixture of light oil and colored pigment. The shearing force of the wind flow acts on the oil film, which traces out the flow direction at the bed. Once the oil evaporates, a pattern is left on the model by the pigment, showing limiting (bed) streamlines, separation, and attachment points. Hunt and Snyder (1980) employed a similar technique in a water channel, using a thick dye solution painted on a model. However, as with $KMnO_4$ the dye separated with the flow and important details were obscured from view.

To investigate in more detail the separation mechanism from shallow conical models and how this changes when the fluid depth is increased, oil-film tests were conducted in a wind tunnel. The models tested were constructed from solid pieces of wood or Perspex, with base diameters of 0.3 m and side slopes ranging from 11.3 to 33.7°. The models were fastened to a 1.2-m-long by 0.6-m-wide plywood base plate supported in the open-jet wind tunnel by a 0.3-m-high angled steel frame. The vertical position of the model was, therefore, toward the center of the working section, away from the strong shear flow of the boundary layers on the wind tunnel walls. The effect of "fluid depth" was produced by using a top plate to act as a "free surface" boundary. The top plate was supported by nuts on threaded rods, fixed at the four corners of the rig. Altering the gap between the plates simulated raising or lowering the flow depth. This differs from a free surface in water, in that a boundary layer will form on the top plate and free surface undulations will not be allowed to occur. When considering separation and attachment points on the surface of the model, the boundary layer formed on the top plate should produce little interference (particularly for moderate to large plate separations) because it is very thin. Observations of flow in the water channel showed there to be little free surface movement. Attempts at measuring the expected free surface dip above the flattened apex of the models proved unsuccessful. The dip was too small to be recorded with confidence, using a point measuring device accurate to ± 0.5 mm.

The models were positioned in the hexagonal working section of the wind tunnel, which had maximum dimensions of 1.1 m (wide) by 0.8 m (high). For all experiments, the mean velocity was set to 10 m/s, with a turbulence intensity measured at around 5%. The Reynolds number based on the mid-height model diameter (≈ 0.15 m) was approximately 1×10^5. This is higher than that used in the water channel studies, where the corresponding Reynolds number was approximately 5×10^4. This relatively high velocity was needed to evaporate the oil in a reasonable timescale of a few minutes and to provide sufficient force for the oil flow droplets to overcome gravity effects. The oil/pigment mixture used for visualization was a combination of kerosine (paraffin oil) and a fine fluorescent powder. An atomizer was used to coat the model with a fine layer of the mixture. Once a visualization test was completed the model was removed from the rig, illuminated with an ultraviolet lamp, and photographed.

Photographs of oil flow visualization tests using a model with a 0.06-m-diameter flattened apex and a 14.0° side slope angle are presented in Figs. 4(a–d). The photographs illustrate the surface patterns produced as h/h_i (where h is now the plate separation) is increased from values that produced a vortex shedding wake (according to hot-wire measurements) to those that did not. It is important to remember that the final flow pattern is a time-averaged representation of what was a highly unsteady flow. Also, the flow at the model surface may be very different to that above it. Features marked by capital letters are referenced in the text. The oil flow patterns produced are complex and, as pointed out by Rosenhead (1963), need to be interpreted with caution. Any discussion relating the patterns to supposed flow phenomena tends to be rather speculative, particularly when the patterns themselves are unclear (some separation-attachment lines were poorly marked).

Fig. 4(a) shows the oil-film pattern produced with $h/h_i = 1.17$ (top plate 5 mm above the model). An interesting feature of this flow pattern is that there appear to be two distinct separation regions. The first occurs from the airflow around the side of the model, separating along lines A and C, with attachment possibly occurring in region B. The accelerated flow above the model does not separate at the edge of the apex plateau as might be expected. In the water channel separation was always observed to occur from this position. This feature of the wind tunnel experiments with small plate separations may have been produced by interference from the boundary layer formed on the top plate and was not observed for larger separations. Separation in this central region downstream of the apex occurs from the line marked D. The link between the separation of the flow around the upper shoulders and that toward the center is unclear, although a form of secondary separation may be occurring along E. Separation from D results in a highly turbulent near-wake region F, with reverse flow on the model surface. The rather streaky appearance of the dye traces in region F is possibly due to the tortuous movement of dye droplets in the turbulent near wake. However, their cell-like structure may indicate some form of organized,

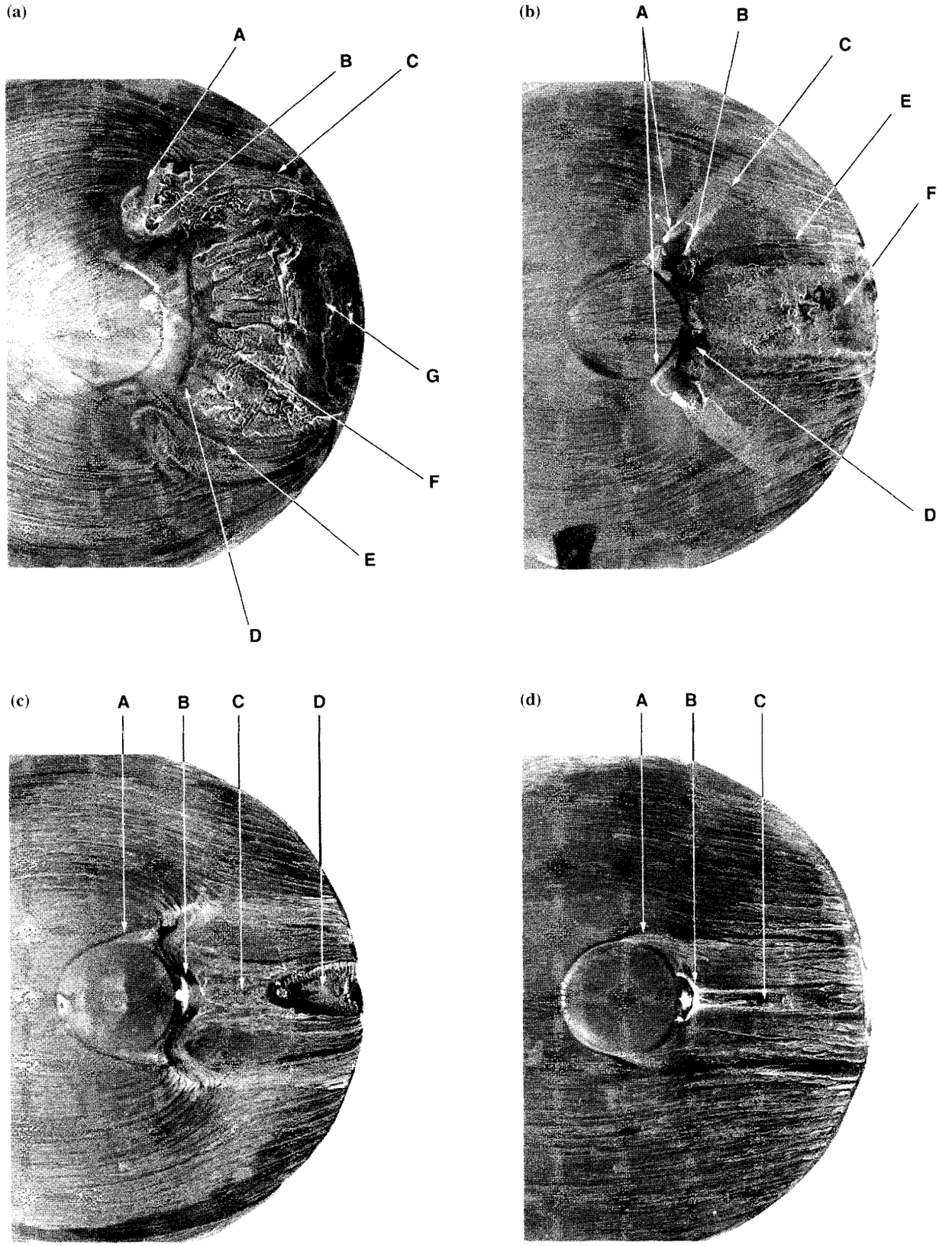

FIG. 4. Photographs of Flow Patterns Produced on Bed of a Conical Model with θ = 14.0° Using Oil-Film Visualization Technique in a Wind Tunnel with Value of h/h_i: (a) 1.17; (b) 1.67; (c) 2.33; (d) Top Plate Removed

longitudinally orientated secondary vortices. The zone marked G shows the formation and shedding region of unsteady vortices. Hot-wire anemometer measurements were taken at a position approximately three middepth diameters downwind of the island center. The measurements indicated a periodic vortex shedding wake with a Strouhal number of 0.35. Measurements at different heights, ranging from 5 to 30 mm above the base plate, showed no variation in frequency, suggesting the wake to be remarkably 2D.

Fig. 4(b) shows the dye pattern produced on the model surface, with the top plate raised to give h/h_i = 1.67 (20 mm above model). The size of the separated regions has clearly

decreased. The lengths of the separation lines around the sides of the model, marked A, are significantly smaller than seen in the previous case with $h/h_i = 1.17$, with a distinctive bubble forming and reattaching at B. The "wing-like" structures protruding from the bubble, marked C, are in positions where separation would be expected. However, the dye traces approaching the upwind edge of these wings show no sign of separation and are seen to pass through this region. The wings appear as a "shadow" of light tracer color and probably indicate weak secondary currents, moving in a direction up toward the bubble. Similar secondary current patterns were observed in the water channel experiments and have been described in foregoing paragraphs. The flow over the apex separates close to the edge of the plateau, probably reattaching in the region marked D. Separation occurs again a short distance downstream, producing a region of reverse flow enclosed by the line E. Zone F suggests an area of unsteady vortex formation. No hot-wire measurements were made for this case, although tests with a steeper model (side slope 22°) measured only weak shedding when the top plate was 20 mm above the island apex. The wake suggested by the pattern marked F has narrowed considerably compared with that found with $h/h_i = 1.17$ in Fig. 4(a).

Raising the top plate further, giving $h/h_i = 2.33$ (40 mm above model), produces the surface flow pattern on the model seen in Fig. 4(c). Flow separating from around the sides does not appear to reattach and form a distinct bubble. A separation/attachment bubble is formed in region B from the flow over the apex. Weak reverse flow occurs in region C, which along with the unsteady region D, has narrowed considerably from the previous case.

With the top plate removed, effectively giving $h/h_i = 13.3$, Fig. 4(d) shows how the unsteady downstream region has disappeared. Separation occurs around the sides (marked A) and from the apex, forming a separation-attachment bubble. No reverse flow occurs along the wake centerline C.

A brief study was made concerning the configuration of the model apex, to investigate the effect this had on the wake flow. In the water channel a peaked conical apex was manufactured and fitted to model 3 ($\theta = 12.6°$). With the use of dye tests the shedding was observed to cease at a similar value of h/h_i to the case with a flattened apex (approximately 1.18 with h_i measured to the apex tip). In the wind tunnel a peaked conical model was also studied with a side slope angle of 11.3°. The h/h_i was varied between 1.17 and 2.33 producing surface patterns very similar to those for the 14.0° model with a flattened apex.

Model Results

All computations were made on a Cray EL98 vector processor. A horizontal square cell size of 0.0152 m and a time step of 0.05 s have been used with all simulations run for 4,000 time steps. For the 2D runs a 328 × 100 horizontal mesh was used. To save central processing unit (CPU) time when running the 3D model, the downstream boundary was moved upstream to give a 218 × 100 horizontal mesh with 20 vertical divisions. A number of 2D runs were made with this reduced horizontal mesh size. The results were very similar to those with 328 × 100 cells, showing the numerical scheme to be insensitive to this change in the boundary condition. With their respective parameter values, a 2D run required approximately 2 h CPU time whereas a 3D run required approximately 50 h CPU time.

For case SB4_01, with $h/h_i = 1.02$, the 2D model produced results that corresponded well with the PTV measurements. The correlation between measured and simulated results is similar to that described in Part I for surface-piercing cases in relatively deep water. This is to be expected with $h/h_i = 1.02$, because there is little flow over the apex and the island acts to shelter the recirculating near-field region. In contrast to the similarities found between the 2D model and experimental flow fields, surface vector plots produced by the 3D model displayed a different vortex structure to the experimental case. Such differences were also a feature of the surface-piercing study. The 3D model includes a relatively simple mixing-length eddy viscosity model for vertical turbulent mixing and is formulated with the hydrostatic pressure distribution. As a consequence, vertical accelerations are neglected and in contrast to experimental observations the amount of vertical mixing produced in the near-field region was relatively small. This weak vertical mixing produced a near wake with a significant depthwise variation in the flow structure. Well downstream of the island, the flow reorganized throughout the depth to give a more 2D field. In the 2D model vertical mixing is effectively instantaneous and thus represents well the rapidly vertical mixing in the near wake observed experimentally.

The flow field produced by the depth-averaged model for case SB4_02 [island 4 ($\theta = 8.0°$) $h/h_i = 1.10$] is illustrated in Fig. 5(a). This is seen to compare reasonably well with the corresponding PTV vector field shown in Fig. 2(b), although in the recirculating region close to the island predicted velocity magnitudes are significantly larger. Experimental and model depth-averaged velocity time histories are compared at measuring stations S1 and S2 in Figs. 6(a and b), respectively. The two measuring stations were 1.02 m downstream of the island center with S1 on the wake centerline and S2 0.27 m away from the centerline. In general the comparison is good, particularly at S2 where the experimental and model mean and peak-to-peak velocities are closely matched. At the centerline position S1, the flow structure is clearly more complex. The peak and mean values of u velocity are greater in the experimental trace, whereas the measured peak v velocity is slightly lower. The shedding frequency produced by the 2D model was 18% higher than the experimental value.

Similar comparisons between the 2D model and experiment were found for runs with depths of $h/h_i = 1.16$ and $h/h_i = 1.20$. Figs. 5(b and c) show the modeled wakes to include features consistent with those measured in the laboratory [see Figs. 2(c and d)] although some differences were apparent in the velocity time history comparisons at positions S1 and S2.

For all four islands the 2D model results were similar, with a vortex shedding wake predicted for small values of h/h_i, weakening with increasing depth. In the laboratory study, a value of h/h_i was reached where shedding with a clear periodic frequency ceased and a narrow, low-velocity wake region formed. This low-velocity wake decayed (i.e., the magnitude of the velocity deficit decreased) slowly as h/h_i increased. In contrast, the 2D model continued to predict a rapid drop in the magnitude of the velocity deficit in the wake for increasing h/h_i. For all runs where shedding occurred, the 2D model overpredicted the dominant frequency. Island 1 ($\theta = 33.1°$) produced the closest match between experimental and numerical results.

The origin of the shedding simulated by the 2D model stems from the high bed-shear stress produced by the shallow accelerated flow near the island apex. The high flow velocity (up to $2.3U_0$ when $h/h_i = 1.10$) produces high shear stresses through the quadratic friction law, with shear stress roughly proportional to velocity squared, which act to deflect the oncoming flow, creating a low-velocity region in the near field. Once this low-velocity region is established, the same mechanism producing vortex shedding in the experiments produces shedding in the simulation (namely, the instability of the horizontal shear layers produced between the low-velocity zone and accelerated flow around the island shoulders). As the flow depth is increased in the 2D model, the magnitude of the bed-

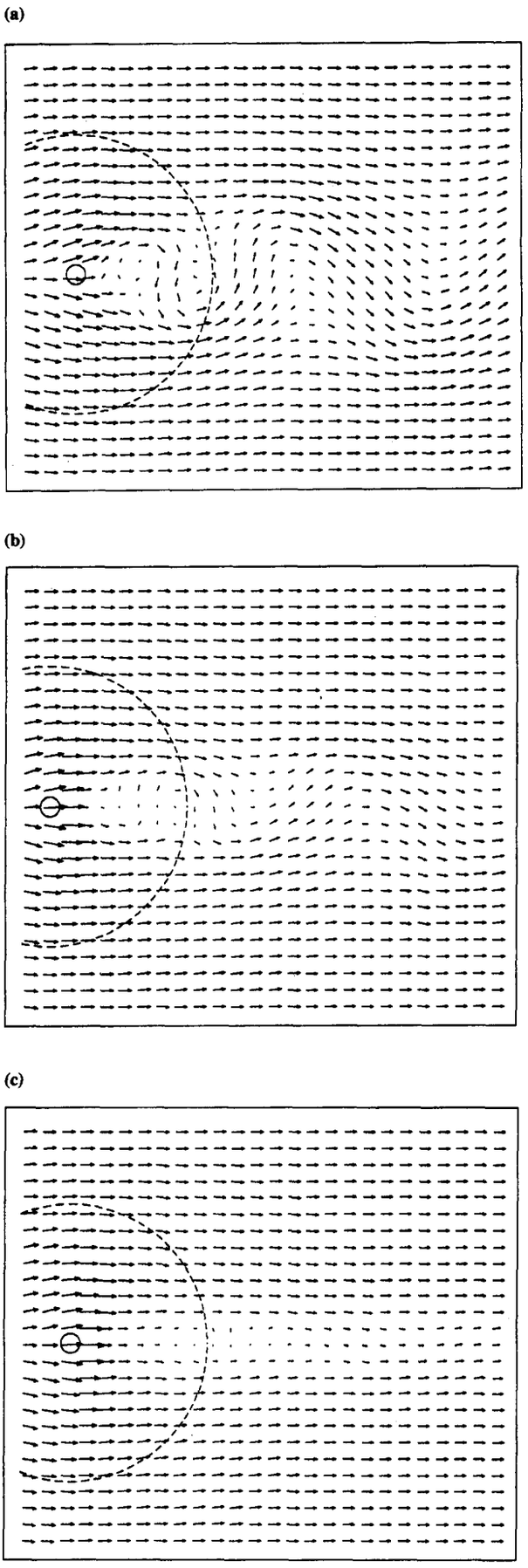

FIG. 5. Depth-Averaged Model Velocity Vector Fields of Wake of Island 4 (θ = 8.0°) with Value of h/h_i: (a) 1.10; (b) 1.16; (c) 1.20

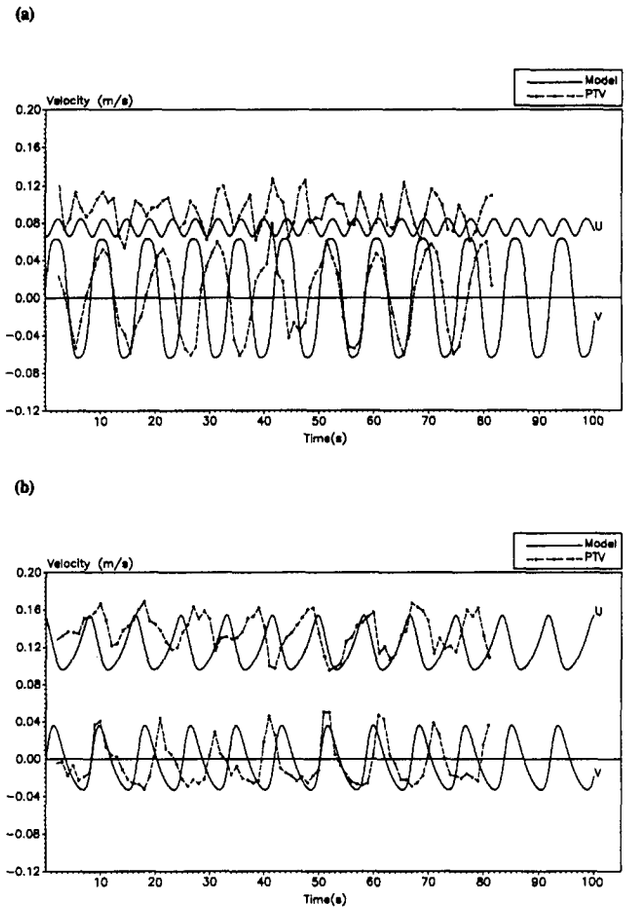

FIG. 6. Variation in Velocities u and v with Time from 2D Computation and Experiment (a) S1, on Wake Centerline; (b) S2, 0.27 m from Wake Centerline

shear stress reduces. This results in greater velocities downstream of the apex producing a narrower and lower-velocity near-field zone. The oscillatory wake weakens correspondingly. For large depths, a narrow steady wake was observed to persist in the experiments. However, once the bed-shear stress is no longer strong enough to affect significantly the flow, the model produces a flow field with wake velocities approaching the free-stream velocity.

In contrast to the 2D model, the 3D model may be expected to reproduce some of the vertical variations observed in the near wake that contributed to the generation of vortex shedding in the experiments. Vector plots of horizontal velocity components are presented at bed, middepth, and free surface positions in Figs. 7(a–c) [island 4 (θ = 8.0°)] for test case SB4_02 with h/h_i = 1.10. Compared with run SB4_01 with h/h_i = 1.02 a more 2D flow is produced in the wake of the island. Vertical mixing, driven by the accelerated flow above the apex, is apparent in Fig. 7(d) showing the u, w velocity components through the central plane. Comparisons of model and experimental surface velocity time histories at positions S1 and S2 are presented in Figs. 8(a and b), respectively, [island 4 (θ = 8.0°), h/h_i = 1.10, measurements 1.02 m downstream of island center]. At S1 the magnitude of the mean predicted u velocity is almost 50% lower than that measured, although the magnitude of the peak v velocities is in good agreement. The length of the recirculating vortex region produced by the 3D model is greater than that observed in the laboratory, almost extending to the measuring position S1 and providing a reason for the lower u velocities. At position S2 the model produces a good representation of the measured velocities. The domi-

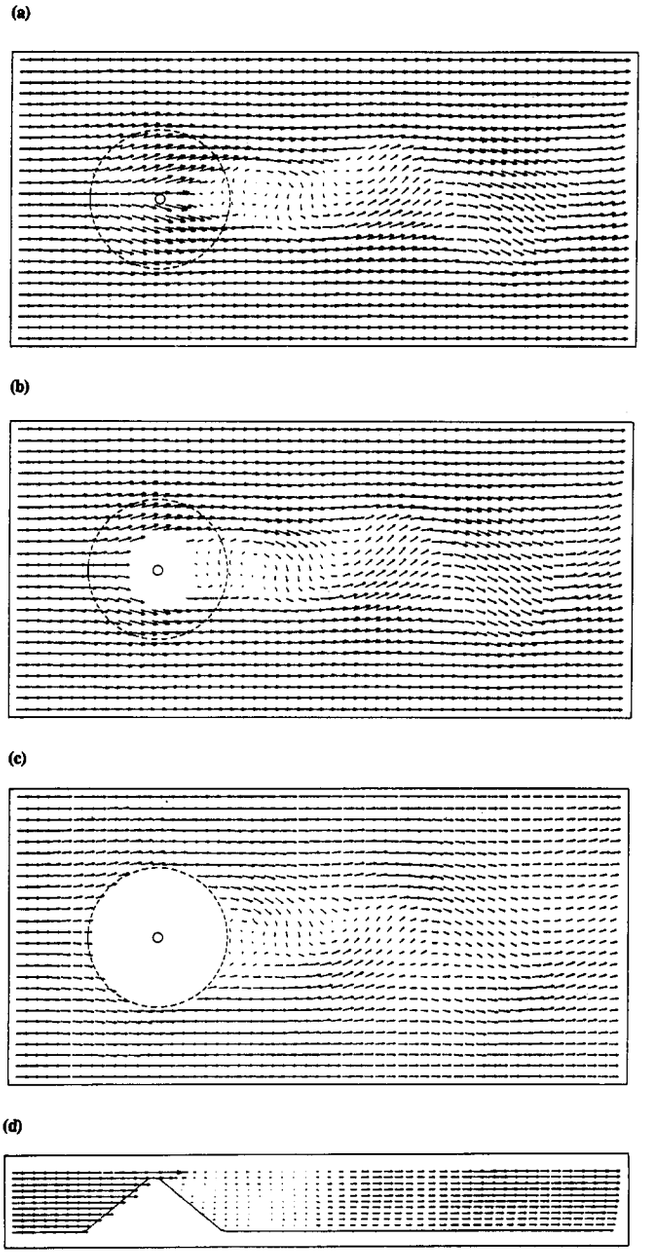

FIG. 7. Velocity Vector Field from 3D Computation: (a) *u*, *v* Velocities at Water Surface; (b) *u*, *v* Velocities at MidDepth; (c) *u*, *v* Velocities at Bed; (d) *u*, *w* Velocities at Mid-*y*-Plane with Depth × 6

nant frequency produced by the model is within 4% of that measured.

Simulations with h/h_i increased to 1.16 and 1.20 produced flow fields that looked very similar to each other. The predicted wakes were wider and contained lower velocity magnitudes than measured in the experiments. This result differs from the 2D model, which predicted higher velocities and a more pronounced wake oscillation than was observed. Weak oscillations are predicted in the wakes approximately two base diameters downstream of the island center.

The 3D model results from flow around the other islands tested in this study (with slopes from 12.6 to 33.1°) were similar to those described above for island 4. Where a recirculating flow region occurred, it tended to be situated further downstream than observed in the laboratory. Mean velocities along the wake centerline were underestimated for all cases. The predicted wake tended to be wider than the experimental one,

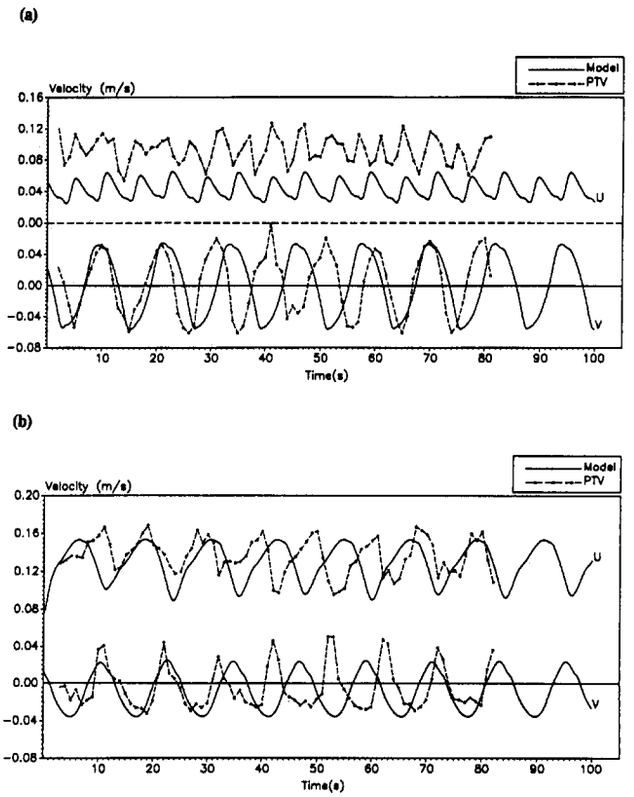

FIG. 8. Variation in Surface Velocities *u* and *v* with Time from 3D Computation and Experiment: (a) S1, on Wake Centerline; (b) S2, 0.27 m from Wake Centerline

accounting for the lower dominant frequencies predicted by the 3D model.

SUMMARY AND CONCLUSIONS

Experiments in a shallow-water flume demonstrated well-organized vortex shedding occurring in the wake of submerged conical islands when the depth above the model apex was relatively small. The shedding was observed behind models with slopes ranging from 8.0 to 33.1°. Observations using dye visualization showed this large-scale, horizontal shedding to be generated by the instability of shear layers, produced between a low-velocity region in the near wake and high-velocity regions across from the apex. Increasing the water depth caused the low-velocity region in the near wake to narrow and the magnitude of the velocity deficit to decrease, resulting in the vortex shedding system becoming less vigorous. At a certain depth ($h/h_i \approx 1.13-1.18$ for the models used here) well-organized shedding stopped. Complementary experimentation was provided by wind tunnel studies. More detailed investigation into the near-wake processes causing vortex shedding would be desirable. In particular, using a laser light sheet to illuminate a vertical 2D slice of the near wake, PTV measurements, using much smaller particles than used in the present study, would provide valuable quantitative velocity information not provided here.

Overall the 2D model produced reasonably good simulations of the submerged island wakes in spite of the 3D nature of the near-wake flow. With $h/h_i = 1.10$, measurements of mean u velocity at far-wake positions were within 15%, although the dominant shedding frequency was overpredicted. For the same test case (SB4_02) the 3D model demonstrated "separation-like" effects in the near wake. This helped to produce a more 2D far wake than was reported in Part I for the surface-piercing simulations. Although the mean u velocity at a position on the wake centerline was underpredicted by 37%,

the dominant shedding frequency predicted by the model was within 5% of the experimental value. With increasing water depth the 3D model was seen to simulate a form of the steady wake similar to those observed in the laboratory, although velocities along the wake centerline were lower than measured in the experiments.

It is perhaps surprising that the 2D model can, in some cases, more accurately simulate experimental wakes than the 3D model. Although the large-scale model wake features resemble those measured in the laboratory their mode of generation can be entirely different. In the 2D model the low-velocity near-wake region is produced only by high bed-shear stress generated by the shallow water above the apex. The 3D model can simulate some coherent structures in the near wake, which produce vertical mixing, but cannot capture the effects caused by the flow separation. Because the generation of the transverse velocity profile is through a different cause in model and experiment, the reasonable reproduction of large-scale wake features in the model must be regarded as rather fortuitous, emphasizing the need for physical model studies for validation purposes.

ACKNOWLEDGMENT

This project was undertaken when Peter Lloyd was in receipt of an Engineering and Physical Sciences Research Council (EPSRC) Marine Technology studentship and we acknowledge this gratefully.

APPENDIX I. REFERENCES

Arya, S. P. S., Capuano, M. E., and Fagen, L. C. (1987). "Some fluid modelling studies of flow and dispersion over two-dimensional low hills." *Atmospheric Envir.*, 21(4), 753–764.

Arya, S. P. S., and Gadiyaram, P. S. (1986). "An experimental study of flow and dispersion in the wakes of three-dimensional low hills." *Atmospheric Envir.*, 20(4), 729–740.

Brighton, P. W. M. (1978). "Strongly stratified flow past three-dimensional obstacles." *Quarterly J. Royal Meterological Society*, Bracknell, U.K., 104, 289–307.

Chen, D., and Jirka, G. H. (1995). "Experimental study of plane turbulent wakes in shallow water." *Fluid Dyn. Res.*, 16, 11–41.

Engel, P. (1981). "Length of flow separation over dunes." *J. Hydr. Div.*, ASCE, 107(10), 1133–1143.

Genin, A., Dayton, P. K., Lonsdale, P. F., and Spiess, F. N. (1986). "Corals on seamount peaks provide evidence of current acceleration over deep-sea topography." *Nature*, 322(3), 59–61.

Hamner, W. M., and Hauri, I. R. (1981). "Effects of island mass: water flow and plankton pattern around a reef in the Great Barrier Reef lagoon, Australia." *Limnol. Oceanography*, 26(6), 1084–1102.

Hunt, J. C. R., and Snyder, W. H. (1980). "Experiments in stably and neutrally stratified flow over a model three-dimensional hill." *J. Fluid Mech.* Cambridge, U.K., 96(4), 671–704.

Huppert, H. E., and Bryan, K. (1975). "Topographically generated eddies." *Deep-Sea Res.*, 23(8), 655–679.

Johns, B. (1991). "The modelling of the free surface flow of water over topography." *Coast. Engrg.*, 15(2), 257–278.

Lloyd, P. M., Stansby, P. K., and Ball, D. J. (1995). "Unsteady surface velocity field measurement using particle tracking velocimetry." *J. Hydr. Res.*, Delft, The Netherlands, 33(4), 519–534.

Nakayama, Y. (1988). *Visualized flow*. The Japan Society of Mechanical Engineers, Pergamon Press, Inc., Tarrytown, N.Y.

Pingree, R. D., and Maddock. L. (1979). "The tidal physics of headland flows and offshore tidal bank formation." *Marine Geol.*, 32(2), 269–289.

Rosenhead, R. (1963). *Laminar boundary layers*. Oxford University Press, New York, N.Y.

Snyder, W. H. (1985) "Fluid modelling of pollutant transport and diffusion in stably stratified flows over complex terrain." *Ann. Rev. Fluid Mech.*, 17, 239–66.

Stansby, P. K., and Lloyd, P. M. (1995). "A semi-implicit Lagrangian scheme for 3-D shallow water flow with a two-layer tubulence model." *Int. J. Numer. Methods in Fluids*, 20(2), 115–133.

Wolanski, E., Pickard, G. L., and Jupp, D. L. B. (1984). "River plumes, coral reefs and mixing in the Gulf of Papua and the Northern Great Barrier Reef." *Estuarine, Coast. and Shelf Sci.*, 18(3), 291–314.

Wood, C. J. (1964). "The effects of base bleed on a periodic wake." *J. of the Royal Aeronautical Soc.*, 68(7), 477–482.

APPENDIX II. NOTATION

The following symbols are used in this paper:

f = dominant wake frequency;
h = water depth or plate separation;
h_i = island height;
R_h = Reynolds number based on water depth;
S = Strouhal number;
T_f = flushing time;
u, v, w = orthogonal x, y, z velocity components;
U_0 = mean free-stream velocity;
x, y, z = orthogonal coordinates;
θ = island side slope angle; and
ν = kinematic viscosity.